Fatigue & Fracture of Engineering Materials & Structures

WILEY

FFEMS Fatigue & Fracture of Engineering Materials & Structures

ORIGINAL ARTICLE

Fatigue Strength Prediction and Degradation Behavior Analysis of 6005A-T6 Aluminum Alloy Considering Fatigue Aging Effects

Bing Yang[1] | Zhe Zhang[1] | Hai Deng[2] | Mingyang Ma[3,4] | Jinbang Liu[1] | Wenyang Shao[1] | Chao Wang[2] | Shoune Xiao[1] | Guangwu Yang[1] | Tao Zhu[1]

[1]State Key Laboratory of Rail Transit Vehicle System, Southwest Jiaotong University, Chengdu, China | [2]Overall R&D Department, CRRC Changchun Railway Vehicles Co., Ltd., Changchun, China | [3]Locomotive & Car Research Institute, China Academy of Railway Sciences Co., Ltd., Beijing, China | [4]Beijing Zongheng Electro-Mechanical Technology Co., Ltd., Beijing, China

Correspondence: Bing Yang (yb@swjtu.edu.cn)

Received: 19 December 2024 | **Revised:** 18 February 2025 | **Accepted:** 13 March 2025

Funding: This work was supported by the National Natural Science Foundation of China (grant numbers 52375159 and 52175123) and the Fund of China Academy of Railway Sciences Corporation Limited (grant number 2022YJ309).

Keywords: 6005A-T6 aluminum alloy | Fatigue aging | Fatigue strength | Mechanical properties | Y-T-F model

ABSTRACT

This study conducts an in-depth analysis of the mechanical property changes of 6005A-T6 aluminum alloy under different fatigue aging states (the process in which the material's performance gradually deteriorates over time under cyclic loading). First, the evolution of surface displacement fields was analyzed using digital image correlation combined with various levels of fatigue aging pretreatment. Through single-cycle tests and tensile tests, the displacement field responses of the material in different degradation states were examined, and changes in ultimate strength, yield strength, elongation, and section shrinkage were further analyzed. Based on the existing yield strength-tensile strength-fatigue strength (Y-T-F) model, an improved approach, the Y-T-F-II model, was proposed to account for fatigue aging effects and validated for fatigue strength prediction, achieving a maximum error of only 0.17%. The results showed that fatigue aging significantly affects the fatigue strength, ductility, and toughness of 6005A-T6 aluminum alloy, and the improved model provides more accurate fatigue strength predictions under various degradation states.

1 | Introduction

The 6xxx series aluminum alloys, due to their excellent forging and plasticity, are widely used in primary load-bearing structures of bridges and other buildings. This material contains magnesium (Mg) and silicon (Si), which give it high strength and excellent corrosion resistance, enabling it to withstand complex external loads and long-term service [1]. For example, the renovation of the first contemporary aluminum alloy road bridge was constructed using extruded profiles of 6082 and 6005 aluminum alloys [2, 3]. As the service life of bridge structures extends, degradation phenomena such as material fatigue [4] and aging gradually emerge, thereby affecting the safety and reliability of the bridge. Therefore, in modern bridge engineering design, it is essential to consider the performance degradation of aluminum alloy materials due to factors such as fatigue and aging during long-term service [5–10].

Existing studies have shown that environmental factors such as temperature [11], vibration, and humidity can lead to fatigue [12], creep, and aging of aluminum alloy materials, thus affecting their mechanical properties, as manifested in the decrease of yield strength, tensile strength, elongation, and other indicators. These changes may lead to the degradation of bridge structural

Summary

- The evolution of material properties of 6005A-T6 during fatigue aging is studied.
- The Y-T-F-II model considering the fatigue aging function of materials is proposed.
- Fatigue aging effects is considered in the tensile-fatigue relationship.
- DIC analysis shows that 6005A-T6 aluminum alloy exhibits cyclic hardening.

performance and even pose potential failure risks [13–17]. Although traditional design methods typically use safety factors to ensure structural safety, for aluminum alloy materials that have already undergone fatigue aging, the bearing capacity of the structure may still be overestimated, increasing the risk of failure [7, 18, 19]. Therefore, considering the degradation behavior of aluminum alloy materials during service, particularly the effects of fatigue and aging, is crucial to ensuring the long-term safety of bridge structures.

A large body of research has been conducted on the properties of aluminum alloy materials. Li et al. [20] investigated the effect of different testing rates on the mechanical properties of 6005A-T6 aluminum alloy, and the results indicated that stress rate does not have a significant impact on strength performance indicators. Peng et al. [21] studied the mechanical behavior of 6005A-T6 aluminum alloy under a strain rate range of 1 s^{-1} to 100 s^{-1}, considering dynamic recovery effects. Their results showed that the strain rate effect on the material was weak at intermediate strain rates. Sun et al. [22] examined the mechanical behavior of 6005A-T6 aluminum alloy under strain rates ranging from 1 s^{-1} to 200 s^{-1}, and obtained similar results. Regarding the study of fatigue crack growth behavior in aluminum alloys, Zhou et al. [23] compared the predictive abilities of four machine learning methods for the fatigue crack growth rate of 6005A-T6 aluminum alloy. They found that the back propagation neural network algorithm demonstrated better performance in extrapolating crack growth rates. Feng et al. [24] applied a physics-informed neural network method to predict the fatigue life of SLM 316L stainless steel. Zhou and Yang [25] used elastoplastic finite element simulation analysis to investigate the effects of different stress ratios and specimen thicknesses on crack growth behavior in 6005A-T6 aluminum alloy. Although these studies have provided in-depth analysis of the basic mechanical properties and fracture behavior of 6005A-T6 aluminum alloy in its unaged state, there is still a lack of research on the effects of fatigue aging on the material.

In the study of material performance parameters after service, Wang et al. [7, 18] used a combined finite element analysis and experimental approach to establish a damage interaction model linked to the physical mechanisms of microstructural evolution, offering an effective nondestructive testing method for aluminum alloys. However, the focus of their discussion was on the evolution of data, without addressing the underlying mechanisms of material performance degradation. Sato et al. [26] studied the cyclic hardening and softening behavior of SN490B structural steel under different loading modes, revealing the influence of strain amplitude on these behaviors. Dinesh et al. [27] investigated the low-cycle fatigue behavior of nickel-based alloy SU-263 at 1023 K, analyzing the effects of strain amplitude on cyclic hardening, softening, and fracture modes. Li et al. [28] studied the dynamic microstructural evolution of GH4169 superalloy under creep-fatigue interaction, proposing a damage assessment method based on the correlation between microstructural degradation and mechanical property degradation, and validating the method's universality. Their research primarily focused on low-cycle fatigue behavior, as the higher loads associated with low-cycle fatigue accelerate material degradation. However, for the aluminum alloy used in bridges, the degradation is typically associated with high-cycle fatigue damage evolution.

Furthermore, research on the correlation between material mechanical properties and fatigue performance has become one of the most effective ways to address the high consumption of fatigue testing [29]. Examples include the relationship between fatigue performance and yield strength [30–32], ultimate strength [32, 33], section shrinkage [34], static toughness [35], as well as hardness [32, 36, 37] and impact toughness [38]. These new models have indeed played a significant role in solving specific problems, but they lack research and analysis on the effects of material fatigue aging on material properties, which further leads to various limitations in the application process. Liu et al. [30] considered both the strength and plasticity limitations of fatigue strength and established a concise relationship between yield strength (Y), tensile strength (T), and fatigue strength (F), which was named the Y-T-F model. Furthermore, in their subsequent study [31], they clarified the direction for improving fatigue strength, which contributes to the optimization of fatigue resistance in metallic materials. Therefore, in the current study, the extent of material fatigue aging will be integrated with the Y-T-F model to enable further analysis.

The literature review indicates that in existing research, comprehensive analysis of the changes in monotonic tensile properties due to material degradation behavior is still lacking, particularly as traditional models fail to adequately consider the impact of fatigue aging on fatigue strength. Therefore, this study first subjected 6005A-T6 aluminum alloy materials to fatigue aging treatments of varying degrees. By spraying a speckle field on the specimen surface and combining it with digital image correlation (DIC) technology, the evolution of the surface displacement field was analyzed. Subsequently, single cycle tests and tensile tests were conducted on 6005A-T6 aluminum alloy specimens in different degradation states to investigate the displacement field response at varying degradation levels, followed by a systematic comparative analysis. An improved method considering the effects of fatigue aging was proposed based on the Y-T-F model, significantly enhancing the accuracy of fatigue strength predictions and validating the effectiveness of this method for fatigue strength prediction under different aging states. Finally, based on the experimental results and fracture observations, the changes in mechanical properties such as ultimate strength, yield strength, elongation, and section shrinkage under different fatigue aging states were analyzed. The material degradation process was further explored through the measurement of surface strain responses.

2 | Experimental Procedure

2.1 | Materials and Specimen Design

The material selected for the experiment is produced 6005A-T6 aluminum alloy, which belongs to the Al-Mg-Si series of heat-treatable aluminum alloys. The filler material for welding is ER5356 welding wire with a diameter of 1.2 mm. The chemical composition of the alloy is shown in Table 1. Although the material selection is for the base material, the welding parameters are still provided, as shown in Table 2. The chemical composition is shown in Table 1. It has moderate strength, as well as excellent extrusion and welding properties, and is widely used in the manufacturing of key components for high-speed train bodies. The specimens were taken from the 10 mm thick base plate region of the welded structure of 6005A-T6 aluminum alloy sheet, as shown in Figure 1. In accordance with the GB/T 228.1-2021 standard [40], the monotonic tensile specimens were prepared using a 0.25 mm diameter molybdenum wire by wire electrical discharge machining (EDM). The dimensional diagram and actual photos are shown in Figure 2c.

To more accurately observe displacement field on the specimen surface, one side of the specimen was polished with silicon carbide sandpaper, while the other side was sprayed with randomly distributed speckles, as shown in Figure 2a.

2.2 | Pre-fatigue, Single-Cycle, and Tensile Tests

All three experiments in this study were conducted on the MTS 809.25 torsional fatigue testing system, using DIC to capture speckle images, with a CCD camera aligned vertically to the specimen. To improve spatial resolution, a macro zoom lens was used for focusing. The speckle pattern on the specimen surface was illuminated by an EFIII-200 LED light source, to facilitate clearer observation of the speckle pattern during image processing. The aforementioned equipment is shown in Figure 2b. Figure 2a shows the clamping method for the specimen, which was used for pre-fatigue, single cycle, and monotonic tensile tests. Image processing was carried out using Revealer 2D-DIC software, with a template size set to 39, grid spacing of 7, and an average spatial calibration resolution of 25 μm/pixel, to achieve the highest displacement map resolution. The analysis employed the multi-point overdetermination method proposed by Sanford and Dally [41], which has been widely used in the analysis of specimen surface displacement fields in photoelasticity or DIC images.

2.2.1 | Pre-fatigue Tests

Pre-fatigue treatment was applied to the monotonic tensile specimens shown in Figure 2c using cyclic loading. Due to time and budget constraints, a representative stress level of 180 MPa was selected for the study. Performance tests under different aging conditions at this stress level were repeated three times to ensure the feasibility of the experiment and the reliability of the data. To mitigate the influence of the stress ratio, a stress ratio of 0.1 was set, with a frequency of 15 Hz, and the load form is shown in Figure 2d. To investigate the fatigue behavior of the material at different aging levels, pre-fatigue tests were conducted for four different aging states. For each aging state, three valid specimens were used to minimize errors and enhance the repeatability of the test results. The corresponding termination load cycles for the four aging states were: 0 cycles, 0.5×10^5 cycles, 1.0×10^5 cycles, and 1.5×10^5 cycles. These pre-fatigue tests effectively evaluate the material's performance degradation at different fatigue cycle counts, allowing for the analysis of its behavior during long-term service.

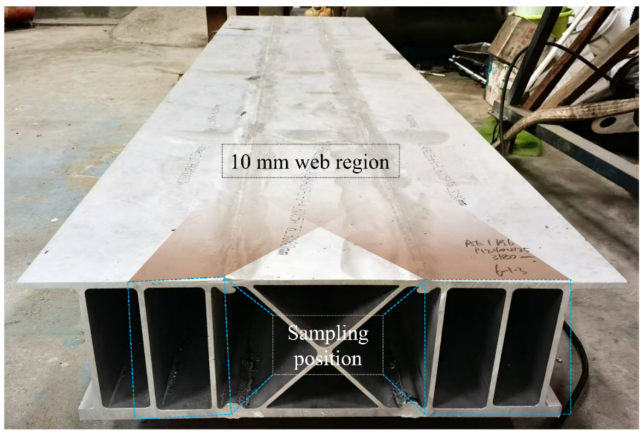

FIGURE 1 | Sampling location of 6005A-T6 aluminum alloy. [Colour figure can be viewed at wileyonlinelibrary.com]

TABLE 1 | Alloy composition of 6005A-T6 aluminum alloy (mass fraction, %) [39].

	Si	Fe	Cu	Mn	Mg	Cr	Zn	Ti	Al
6005A-T6	0.75	0.35	0.30	0.50	0.60	0.30	0.15	0.10	Balance
ER5356	0.10	0.40	0.10	0.15	4.80	0.10	0.10	0.13	Balance

TABLE 2 | Composite welding process parameters [39].

Welding speed	Feeding speed	Laser power	Gas flow rate	Electric current	Voltage
8 mm/s	13 m/min	3500 kW	40 L/min	220 A	23 V

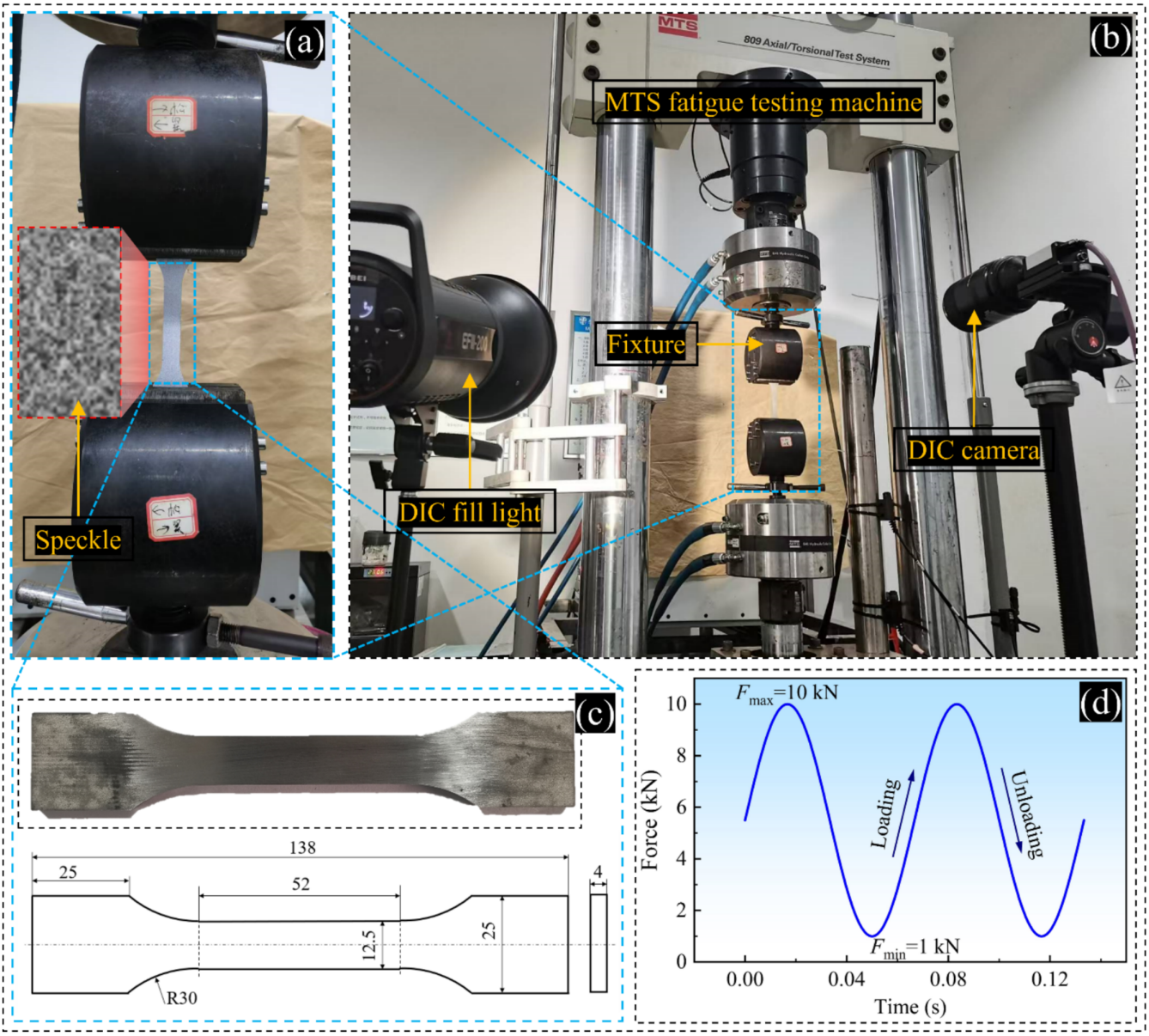

FIGURE 2 | Pre-fatigue, single cycle, and monotonic tensile testing equipment. (a) Specimen fixture. (b) Testing equipment. (c) Specimen dimensions (unit: mm). (d) Pre-fatigue and single cycle load-displacement curves [Colour figure can be viewed at wileyonlinelibrary.com]

2.2.2 | Single-Cycle Tests

After completing the pre-fatigue tests, single-cycle loading tests were conducted on specimens with different aging states to investigate the effect of aging level on the displacement and strain fields of the specimen surface within the same load range. Each single-cycle loading was paused at a fixed load position to manually capture 13 images for subsequent DIC analysis. In the DIC analysis, the image captured at the minimum load of the cycle was set as the reference image, and the image captured at the maximum load was set as the target image. The DIC analysis allows for the calculation of the strain field variations, enabling detailed observation of the changes in the specimen's surface strain during a single cycle. This process is crucial for gaining a deeper understanding of the deformation characteristics of the material in different aging states.

2.2.3 | Tensile Tests

After completing the pre-fatigue treatment and single-cycle loading tests, monotonic tensile tests were conducted on specimens with different aging states, according to the GB/T 228.1-2021 standard [40]. The tensile tests were performed using a displacement control mode with a rate of 1 mm/min. During the test, the same DIC equipment was used to capture speckle images at a frequency of 1 Hz. By analyzing the obtained speckle images, the changes in the surface displacement field of the specimen during tensile testing can be acquired. Furthermore, combined with the analysis of the stress–strain curve, the effect of different aging states on the material's mechanical properties (such as yield strength, ultimate strength, elongation) was investigated. This part of the experiment provided crucial experimental data for the subsequent investigation of

the material's mechanical performance degradation during long-term service.

3 | Results and Discussion

3.1 | Microstructure of Materials

Figure 3 shows the microstructure and inverse pole figure (IPF) of the base material region of 6005A-T6 aluminum alloy. Figures 3a to 4c present the IPFs in three directions, showing the grain orientation distribution in the aluminum alloy base material. In these figures, the color variations of the grains represent the distribution of different grain orientations, and this orientation information reflects the texture characteristics of the material. After rolling, the grain orientation of the base material significantly aligns with the [001] direction along the *Y*-axis, which is characteristic of the rolling process. This indicates that the grain orientation of the material was notably influenced by external forces during the rolling process. Figure 3d is a microstructure image showing the microscopic structure of the 6005A-T6 aluminum alloy matrix. A certain amount of dispersed phase particles can be observed in the aluminum alloy, which are typically precipitates of alloying elements. These dispersed phases may influence the material's strength and toughness.

3.2 | Fracture Analysis

The fracture surfaces of the 6005A-T6 aluminum alloy material under each aging condition were observed and analyzed using the SEM5000X field emission scanning electron microscope from CIQTEK Co., Ltd. Figure 4 shows the macro and micro fracture surfaces of the samples under different aging states. As seen from the figure, in the newly fabricated (0 cycles) state, the fracture surface is relatively smooth with deep and uniform ductile dimples in the microstructure, indicating good material toughness and strong plastic deformation ability. After 0.5×10^5 cycles of fatigue loading, larger ductile dimples appear on the fracture surface, which is the result of the initial fatigue cycles increasing the dislocation density within the material and causing plastic hardening effects in the microstructure.

However, as the fatigue cycles further increase to 1.0×10^5 cycles, the ductile dimples on the fracture surface gradually become smaller, exhibiting rough and uneven characteristics. This change in fracture characteristics is consistent with the slight increase in yield strength, indicating that the strain hardening effect becomes saturated at this stage and the plastic deformation capacity within the material is limited.

In the 1.5×10^5 cycles aging state, the ductile dimples on the fracture surface are noticeably shallower, with penetrating cracks and numerous micropores, indicating a significant increase in the material's brittleness. At this point, the expansion of microcracks causes the ductile dimples to connect and form through-thickness damage. This change in fracture characteristics indicates that the material's ductility and toughness have significantly degraded, which is consistent with the trend of increasing ultimate strength. It can be inferred that the increase in the material's tensile strength is primarily due to the expansion and connection of microcracks and the local deformation behavior they induce, rather than a true improvement in the material's plasticity or ductility.

The combined experimental results and fracture surface features show that during the early stages of fatigue, the material's yield strength and ultimate strength increase due to strain hardening. However, the microstructure gradually degrades, leading to shallower ductile dimples and increased brittleness. This change in fracture characteristics reveals the degradation mechanism of the material's performance under fatigue cycling, which involves the gradual loss of plasticity, ultimately leading to the deterioration of the material's structural performance.

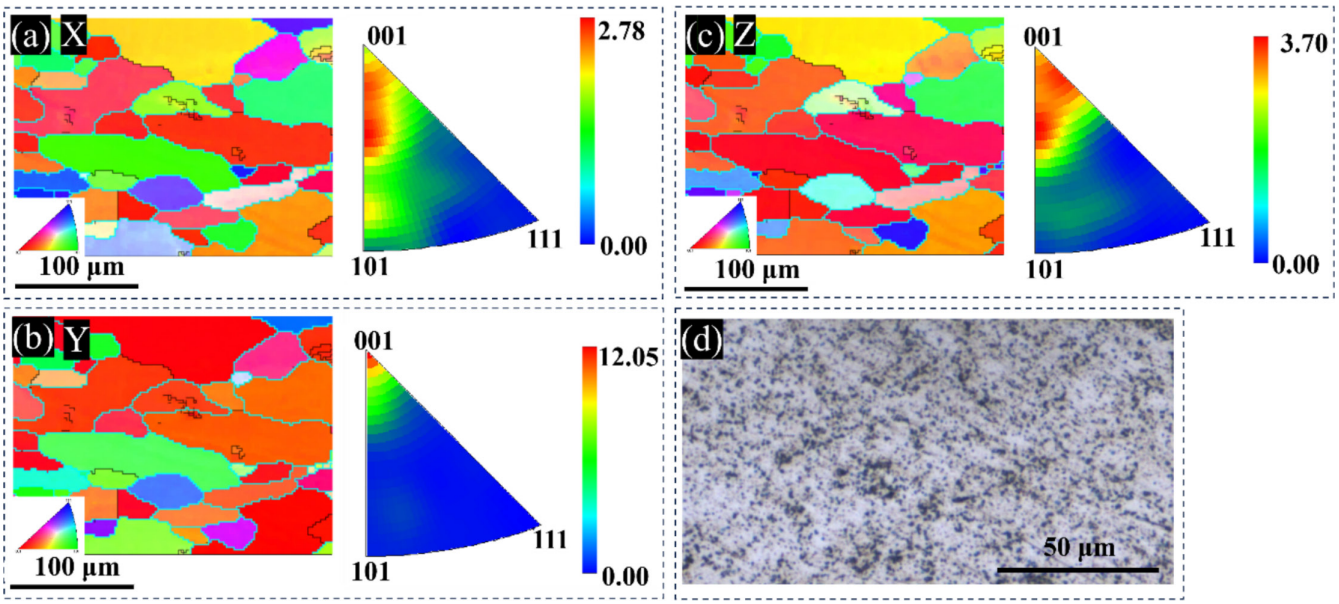

FIGURE 3 | IPF and microstructure of the 6005A-T6 aluminum alloy base metal (BM) region. (a), (b), and (c) are the IPFs in the *X*, *Y*, and *Z* directions, respectively [39], and (d) is the microstructure. [Colour figure can be viewed at wileyonlinelibrary.com]

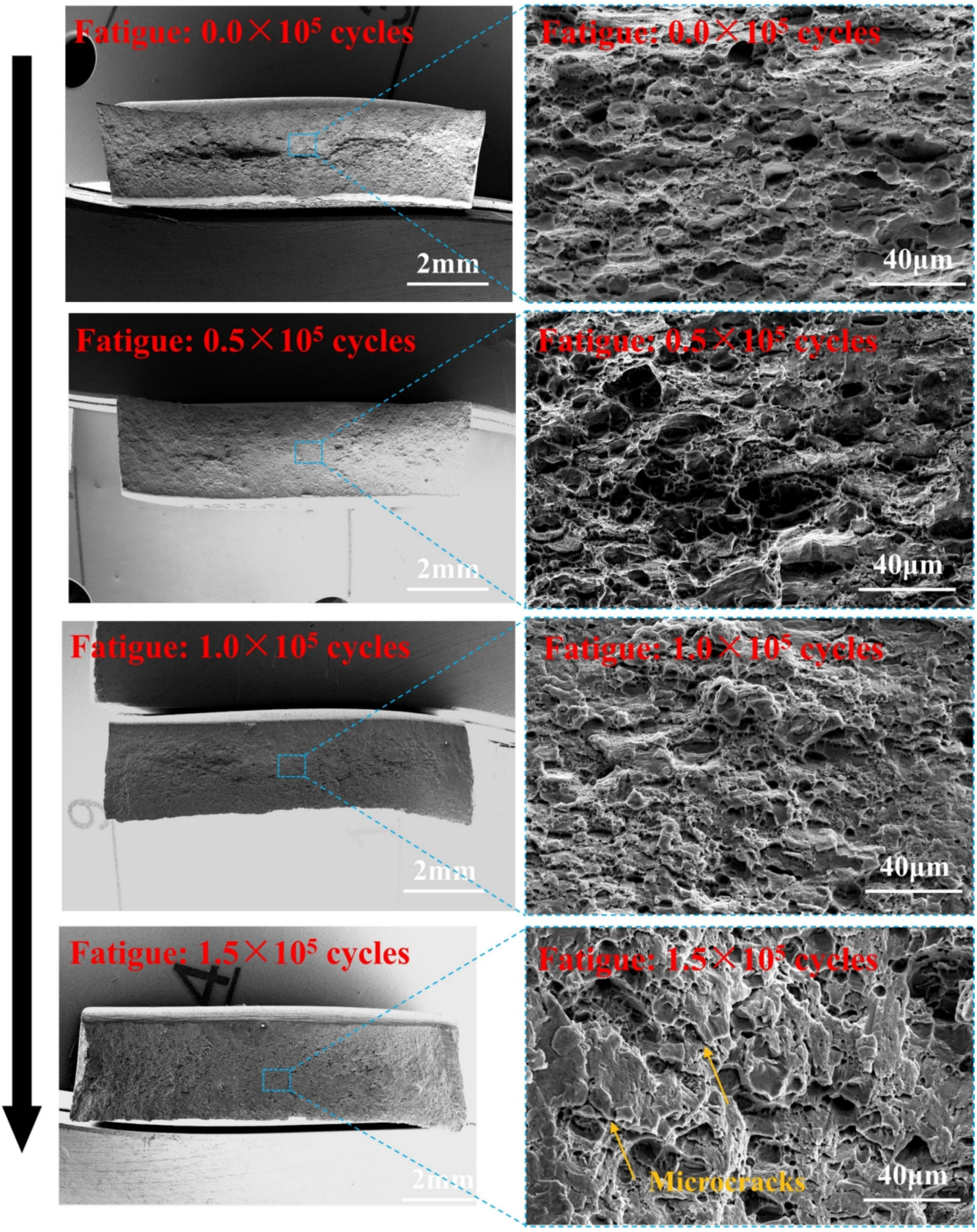

FIGURE 4 | Fracture analysis of the samples under different aging states. [Colour figure can be viewed at wileyonlinelibrary.com]

3.3 | Monotonic Tensile Properties Under Different Aging States

Table 3 and Figure 5 present the monotonic tensile performance parameters, tensile curves, and strain responses of 6005A-T6 aluminum alloy under different aging states, respectively. The section shrinkage refers to the difference between the cross-sectional area at the necking region and the original cross-sectional area, divided by the original cross-sectional area. As shown in the figures and table, the monotonic tensile curves of 6005A-T6 aluminum alloy specimens under different aging states exhibit consistent overall trends. They all display typical tensile characteristics, starting with a linear elastic phase, followed by a yield plateau, and ultimately reaching fracture. These curves demonstrate high repeatability and consistency, particularly in terms of yield strength and tensile strength. The trends of curve variations under each aging state are similar, and their numerical values are closely aligned. Additionally, the tensile curves of specimens subjected to different fatigue cycle counts (such as 1.0×10^5 cycles and 1.5×10^5 cycles) exhibit similar morphologies and yield behaviors, indicating consistency in tensile performance under the experimental conditions. Overall, the experimental results show high repeatability and good consistency in the morphology of the tensile curves, indicating strong stability in the experimental design and operational processes. This provides a reliable foundation for further analysis of the impact of different fatigue states on the mechanical properties of the material during long-term service.

The strain responses at points A, B, C, and D in Figure 5 clearly illustrate the different stages of the tensile deformation process and correspond to the strain distribution maps. This demonstrates the stress–strain behavior characteristics of the material under various aging states. From the initial stage of linear elastic deformation to the stress concentration in the yield phase, and finally to the stress release at fracture, the strain distribution in each stage reflects the influence of aging states on the internal stress transmission within the material.

Table 4 and Figure 5 present the average tensile properties of 6005A-T6 aluminum alloy under different aging states. For new materials, the average tensile strength, yield strength, section shrinkage, and elongation are 222.00 MPa, 270.67 MPa, 34.05%, and 12.18%, respectively. Figure 6 illustrates the trends and fitted curves of monotonic tensile performance parameters for effective specimens under different aging states. According to the data in the figures and table, in Figure 6a, as the degree of aging increases, the section shrinkage shows a decreasing trend, indicating a gradual weakening of the material's toughness, which follows the same trend as the experimental results of Ye [42]. This may be due to cumulative damage caused by cyclic loading within the material, such as the formation and propagation of microcracks [43, 44]. Although the maximum cyclic load is below the yield strength, repeated cycles lead to an increase in internal microscopic defects, reducing the material's plastic deformation capability and resulting in a decreased section shrinkage. Based on the section shrinkage of specimen BM13, it can be inferred that the specimen is approaching fatigue failure after aging, exhibiting significantly lower plastic deformation capability and a marked decrease in section shrinkage.

In Figure 6b, as the aging degree increases, there is a slight increase in elongation. Combined with the fracture analysis in Figure 4, it can be seen that the increase in elongation does not indicate an improvement in the material's plasticity or ductility, but rather reflects the stretching behavior before crack propagation and localized fracture. This phenomenon actually indicates that the material tends to embrittle during the fatigue aging process, with crack propagation paths dominating the fracture process. Therefore, it does not represent an enhancement of material plasticity, but rather manifests as brittle fracture characteristics. Moreover, a substantial

TABLE 3 | Monotonic tensile performance parameters under different aging states.

Specimen no.	Aging states N^{pre} /$\times10^5$ cycles	Yield strength σ_y/MPa	Ultimate strength σ_b/MPa	Section shrinkage Ψ	Elongation δ
BM1	0.0	228	277	33.22%	11.92%
BM2	0.0	218	264	37.18%	12.50%
BM3	0.0	220	271	31.76%	12.12%
BM16	0.5	235	280	31.84%	12.69%
BM17	0.5	232	279	32.92%	13.46%
BM18	0.5	237	275	31.05%	13.08%
BM6	1.0	236	279	33.76%	14.42%
BM7	1.0	241	284	31.68%	14.04%
BM8	1.0	232	273	29.22%	13.85%
BM11	1.5	233	274	31.01%	14.42%
BM12	1.5	237	280	29.69%	14.62%
BM13	1.5	242	285	18.10%	14.71%

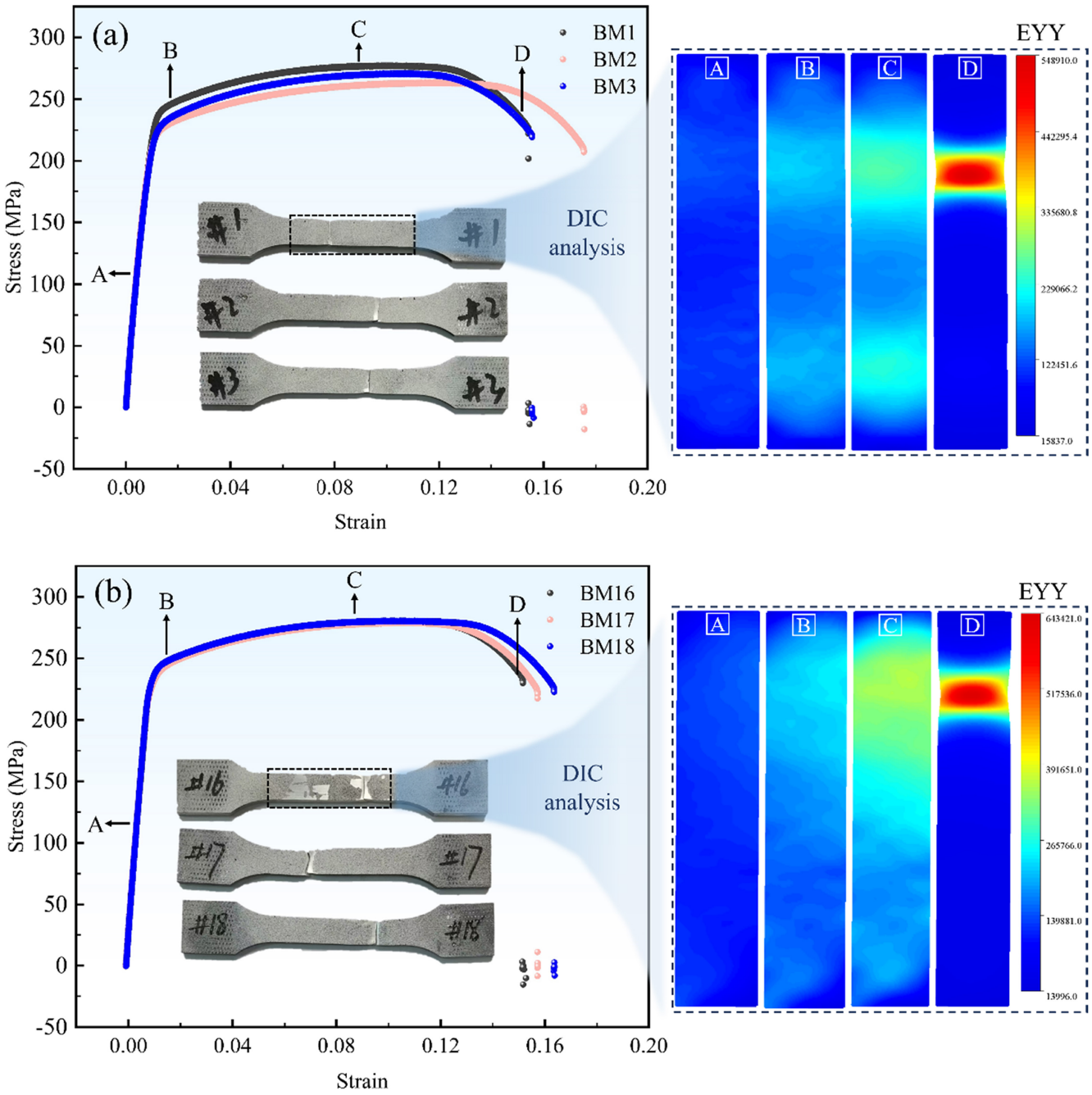

FIGURE 5 | Legend on next page.

amount of literature has reported changes in the elongation of metal materials after fatigue loading under different loading conditions [45–48].

In Figure 6c, as the aging degree intensifies, the yield strength shows a slight increasing trend. During the initial stage of aging, the yield strength rapidly increases, which may be due to a rapid rise in dislocation density within the material under cyclic loading, leading to a significant enhancement of the strain hardening effect. In the early stages of cyclic loading, the increase in dislocations, their interactions, and the formation of slip planes hinder dislocation movement, resulting in a noticeable "dislocation pinning" phenomenon that further elevates the yield strength. The accumulation of dislocations in this phase is relatively rapid, resulting in a rapid rise in yield strength. However, as the degree of aging further intensifies, dislocations gradually reach a saturation state, and the incremental interactions between dislocations slow down, causing the rate of increase in yield strength to decelerate. In other materials, different trends may be observed. For example, the yield stress of AISI 4140 T steel significantly decreases after experiencing fatigue loading [49].

In Figure 6d, as the aging degree intensifies, the tensile strength also increases with aging, indicating that the material exhibits stronger tensile performance after being subjected to cyclic loading. The accumulation of dislocations and the strain hardening effect induced by cyclic loading enhance the material's tensile strength.

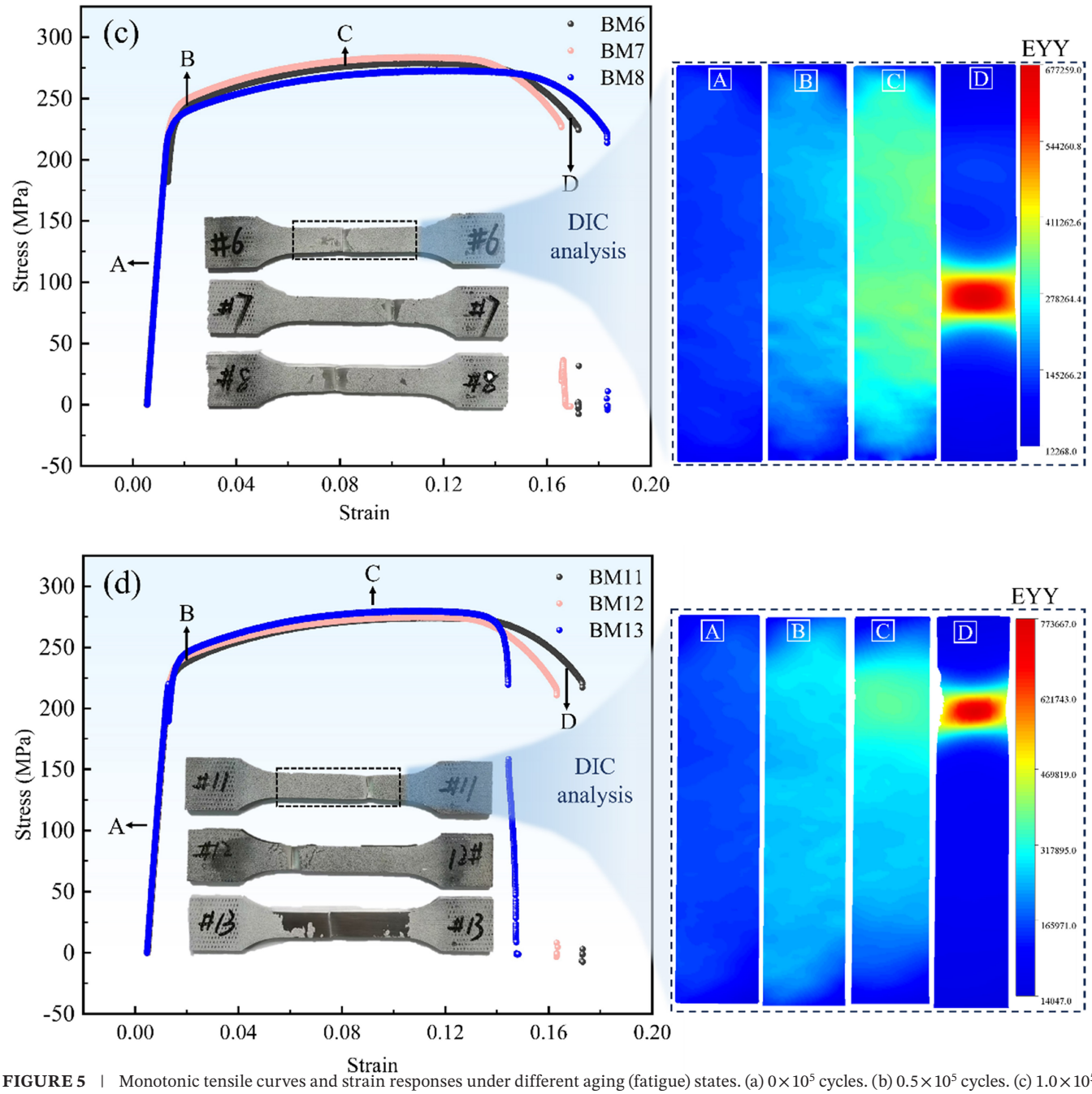

FIGURE 5 | Monotonic tensile curves and strain responses under different aging (fatigue) states. (a) 0×10^5 cycles. (b) 0.5×10^5 cycles. (c) 1.0×10^5 cycles. (d) 1.5×10^5 cycles [Colour figure can be viewed at wileyonlinelibrary.com]

TABLE 4 | Mean values of monotonic tensile properties under different aging states.

Aging states N^{pre} /$\times10^5$ cycle	Yield strength σ_y/MPa	Ultimate strength σ_b/MPa	Section shrinkage Ψ	Elongation δ
0.0	222.00	270.67	34.05 %	12.18 %
0.5	234.67	278.00	31.94 %	13.08 %
1.0	236.33	278.67	31.55 %	14.10 %
1.5	237.33	279.67	26.27 %	14.58 %

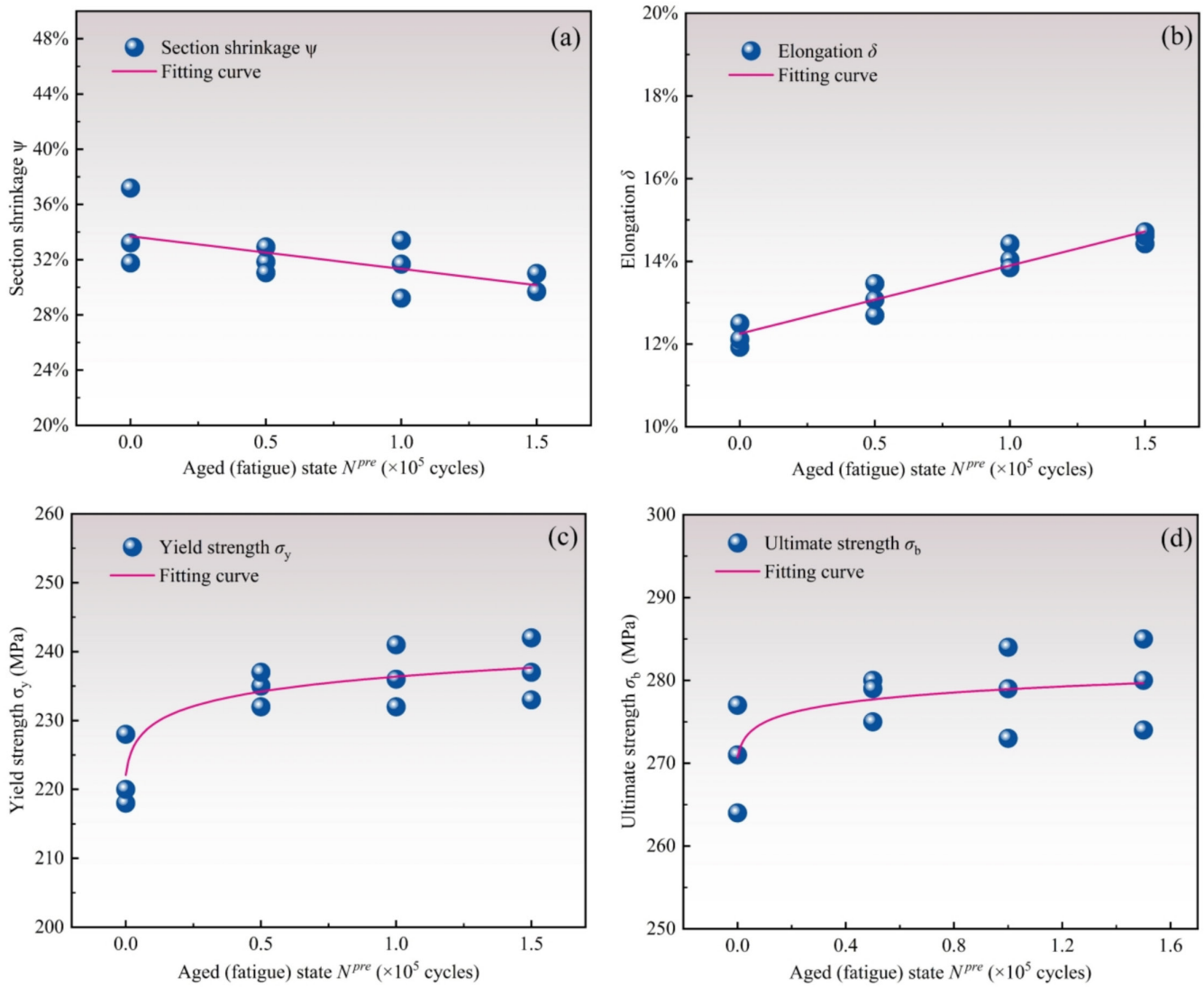

FIGURE 6 | Variation trend of monotonic tensile properties and fitting curves of effective samples under different aging states. (a) Section shrinkage. (b) Elongation. (c) Yield strength. (d) Ultimate strength [Colour figure can be viewed at wileyonlinelibrary.com]

The trend of the monotonic tensile performance parameters for the effective specimens under different fatigue aging states in Figure 6 was fitted using the least squares method, yielding Equations (1)~(4):

$$\Psi = -0.0236 \times 10^{-5} \cdot N^{pre} + 0.3370 \tag{1}$$

$$\delta = 0.0165 \times 10^{-5} \cdot N^{pre} + 0.1225 \tag{2}$$

$$\sigma_y = 236.3396 \times \left(10^{-5} \cdot N^{pre} + 0.0100\right)^{0.0135} \tag{3}$$

$$\sigma_b = 278.9133 \times \left(10^{-5} \cdot N^{pre} + 0.0100\right)^{0.0065} \tag{4}$$

where Ψ represents the section shrinkage; δ represents the elongation; σ_y represents the yield strength; σ_b represents the ultimate tensile strength; and N^{pre} represents the number of fatigue cycles experienced in the given aging state.

3.4 | Fatigue Strength Calculation Model Considering Aging States

Since Wöhler [50] proposed the proportional relationship between fatigue strength and yield strength/tensile strength around 1870, the relationship between the tensile properties and fatigue performance of materials has gradually been revealed. Fan et al. [51], through the study of Pearson correlation coefficients between five input features and fatigue strength, also observed a strong correlation between tensile strength, yield strength, and fatigue strength, as shown in Figure 7. Therefore, this correlation can be used to establish a relationship between the degree of fatigue aging and fatigue strength, and further explore the impact of fatigue aging on fatigue strength.

Traditional fatigue prediction models are typically based on the relationship between fatigue strength and tensile strength or hardness [29]. The relationship between the tensile strength

and fatigue strength of aluminum alloys also follows the Wöhler criterion as shown in Equation (5) [50]:

$$\frac{\sigma_w}{\sigma_b} = A \tag{5}$$

where σ_w represents fatigue strength at a specific stress ratio and failure cycle count (in this study, the stress ratio is 0.1, and the number of cycles to failure is 10^7); σ_b represents the ultimate tensile strength; and A is the material constant. As shown in Figure 8, the constant A for aluminum alloys ranges from 0.3 to 0.5, with a value of 0.5 adopted in this study [51].

Li et al. [34] presented another relationship between ultimate strength and fatigue strength, as shown in Equation (6).

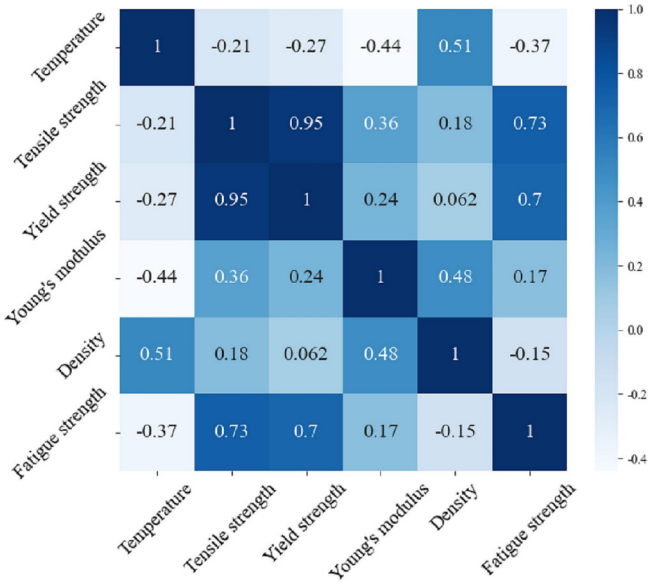

FIGURE 7 | Pearson correlation coefficients between input features and fatigue strength [51]. [Colour figure can be viewed at wileyonlinelibrary.com]

Recently, the Y-T-F model proposed by Liu et al. [30, 31] represents a notable study, as shown in Equation (7):

$$\sigma_w = 1.13 \cdot \sigma_b^{0.9} \tag{6}$$

$$\sigma_w = \frac{\sigma_y}{w}\left(C - \frac{\sigma_y}{\sigma_b}\right) \tag{7}$$

where C and w are the fitted material parameters.

In Equations (5)~(7), it is clear that the purpose of these formulas is to calculate the fatigue strength, which is difficult to obtain, by using material properties such as yield strength and tensile strength, which are easier to measure. The focus of our study is to incorporate the consideration of different material fatigue aging degrees into this process. Analysis indicates that, as shown in Figure 6, with the increase in fatigue aging, both the yield strength and ultimate strength of the material undergo significant nonlinear changes. These changes directly affect the accuracy of fatigue strength predicted by Equation (7). Particularly, when the material undergoes prolonged fatigue cycles, its mechanical properties may change, resulting in simple models being unable to accurately reflect the actual situation. Therefore, relying solely on existing fatigue strength prediction models (such as Equation (7)) may not fully account for the impact of aging effects on fatigue strength. To improve prediction accuracy, the degree of material aging needs to be further considered.

By substituting Equations (3) and (4) into Equations (5)~(7), Equations (8)~(10) can be derived, resulting in Wöhler's law, Li's model, and the Y-T-F model that consider the impact of fatigue aging on material performance. This allows for more accurate prediction of the fatigue strength of 6005A-T6 material in different aging states. Through this improved method, the fatigue life of the material can be better assessed during its design and use, particularly under long-term service or high-cycle fatigue conditions.

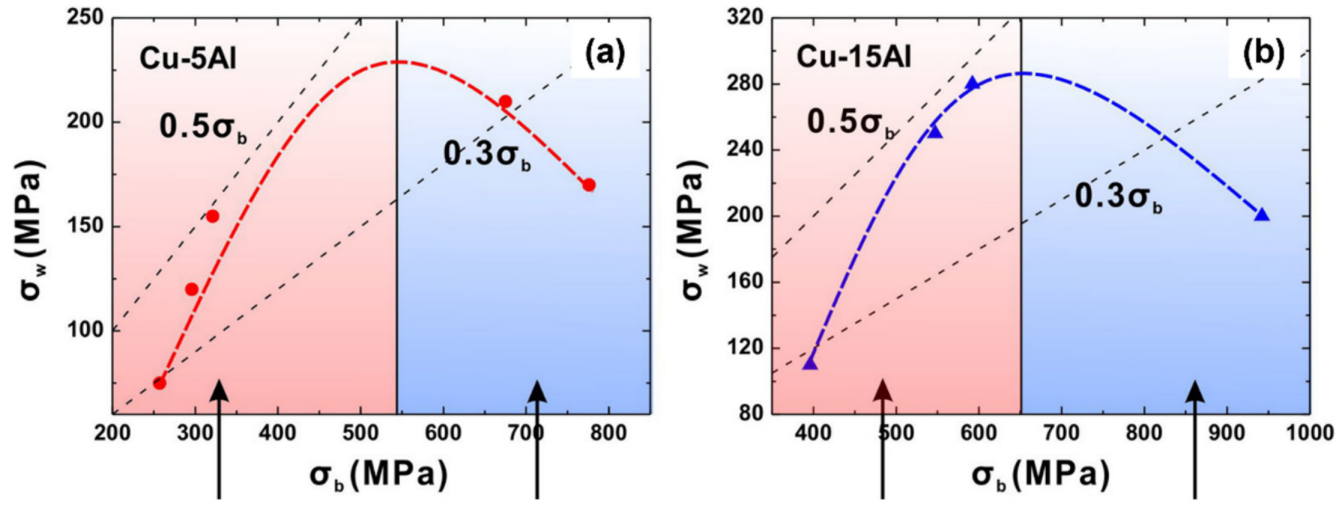

FIGURE 8 | Relationship between ultimate strength and fatigue strength of aluminum alloys [30, 52–54]. [Colour figure can be viewed at wileyonlinelibrary.com]

$$0.5 = \frac{\sigma_{\mathrm{w}}^{pre}}{278.9133 \times \left(10^{-5} \cdot N^{pre} + 0.0100\right)^{0.0065}} \tag{8}$$

$$\sigma_{\mathrm{w}}^{pre} = 1.13 \cdot \left[278.9133 \times \left(10^{-5} \cdot N^{pre} + 0.0100\right)^{0.0065}\right]^{0.9} \tag{9}$$

$$\sigma_{\mathrm{w}}^{pre} = \frac{236.3396 \times \left(10^{-5} \cdot N^{pre} + 0.0100\right)^{0.0135}}{w \left(C - 0.8474 \cdot \left(10^{-5} \cdot N^{pre} + 0.0100\right)^{0.0070}\right)} \tag{10}$$

where $\sigma_{\mathrm{w}}^{pre}$ represents the fatigue strength considering material fatigue aging, defined as the Y-T-F-I model.

Based on the data from different aging states in Table 3, the parameters of Equation (10) were fitted using the least squares method to obtain the constants C and w for different aging degrees.

To further verify the accuracy of the three improved models, the fatigue strengths of different aging states in Table 3 were predicted using the three methods from Equations (8)~(10), with the results shown in Figure 9. It is evident from the figure that the predictions of the improved Li's model are generally higher than the experimental results, while the predictions of the improved Wöhler's law are generally lower than the experimental results. This discrepancy may be due to the fixed calculation parameters in both models, which still lead to some deviation even after considering the effect of material fatigue aging. In contrast, the predictions of the Y-T-F-I model are closer to the experimental results, indicating that this model performs better in fatigue strength prediction. Therefore, the improved Li's model and improved Wöhler's law will not be considered in subsequent studies. It should be noted that for the calculation of experimental fatigue strength of 6005A-T6 aluminum alloy under different aging states, it is sufficient to add the aging cycle count to 10^7 cycles, and then the experimental fatigue strength for different aging levels can be obtained through the SN curve.

However, there is a significant inconsistency in the Y-T-F-I model's predictions. As the material aging degree increases, it is well known that the material's fatigue strength decreases, which is also reflected in the experimental results. However, the predictions of the Y-T-F-I model show an increasing trend. This is because the original Y-T-F model was built based on the positive correlation between the mechanical and fatigue properties of newly produced materials considering different alloy contents (e.g., aluminum content in aluminum alloys). However, under cyclic loading, 6005A-T6 aluminum alloy undergoes cyclic hardening, which improves its mechanical properties. This results in a fatigue strength evolution trend under different aging states that does not align with the actual behavior. Therefore, by introducing an aging function, as shown in Equation (11), the predicted fatigue strength trend under different aging states can be made to align with the experimental trend.

$$\sigma_{\text{w-aging}}^{pre} = \frac{236.3396 \times \left(10^{-5} \cdot N^{pre} + 0.0100\right)^{0.0135}}{w \left(C - 0.8474 \cdot \left(10^{-5} \cdot N^{pre} + 0.0100\right)^{0.0070}\right)} \cdot A(\alpha, \beta) \cdot \tag{11}$$

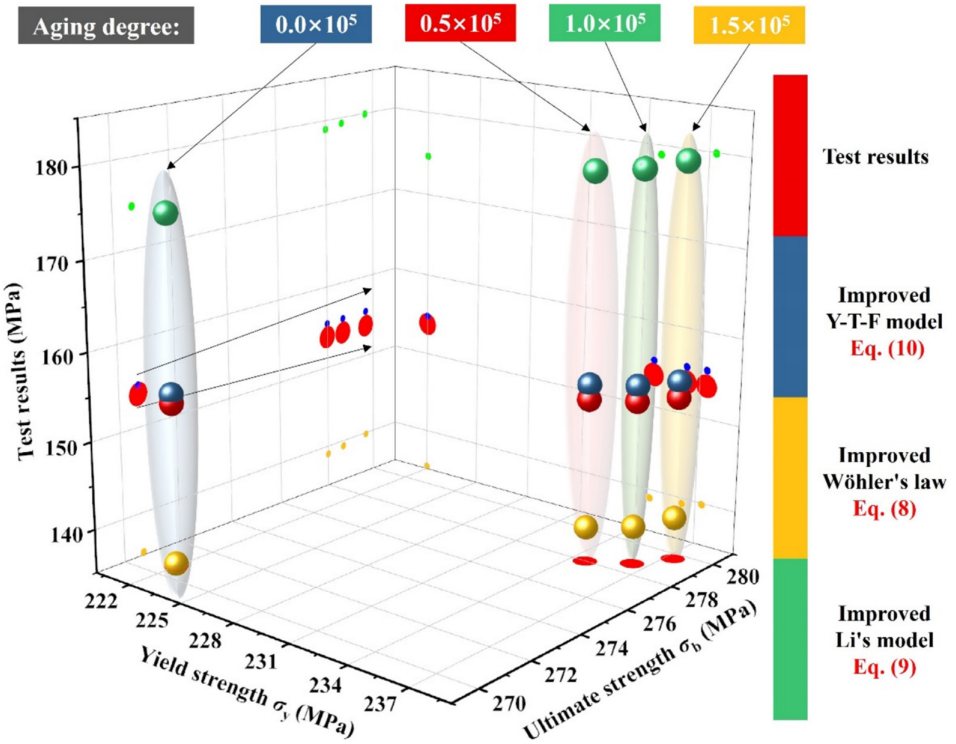

FIGURE 9 | Comparison of the predicted fatigue strength results between the Y-T-F-I model (Equation 10), improved Li's model (Equation 9), and improved Wöhler's law (Equation 8). [Colour figure can be viewed at wileyonlinelibrary.com]

where $\sigma^{pre}_{\text{w-aging}}$ represents the fatigue strength predicted by the improved Y-T-F model with the introduction of the aging function, defined as the Y-T-F-II model; $A(\alpha, \beta)$ is the fatigue aging correction function, obtained through fitting.

Based on this, the experimental results were compared with the predicted fatigue strength results of the Y-T-F-I model (Equation 10) and Y-T-F-II model (Equation 11), as shown in Figure 10. It can be observed that the predictions of the improved Y-T-F-II model, which incorporates the aging correction function, align well with the experimental results.

To further analyze the predictive performance of the models, we compared the prediction errors of the two improved models, as shown in Figure 11. From the error comparison, it is evident that the maximum prediction errors obtained using the Y-T-F-I model and Y-T-F-II model are 2.91% and 0.17%, respectively. This indicates that the Y-T-F-II model predicts fatigue strength more accurately and fully accounts for the impact of material aging. Therefore, for the 6005A-T6 aluminum alloy, the fatigue strength predictions using the Y-T-F-II model, which incorporates the aging function, are more reliable.

3.5 | Single-Cycle Strain Response Under Different Aging States

Figure 12 shows the changes in the displacement field and the *Y*-direction (loading direction) strain field at maximum load relative to zero load under different fatigue aging states during a single cycle. As the fatigue cycles increase, from newly fabricated (0 cycles) to aged (1.5×10^5 cycles), the displacement and strain responses gradually weaken, with the color changing from warm tones to cool tones. This indicates a decrease in the material's deformation amplitude, exhibiting characteristics of cyclic hardening. Combined with the fracture analysis in Figure 4, it is shown that as fatigue accumulates, the dislocation density within the material increases, and the entanglement and interaction between dislocations intensify, limiting the material's plastic deformation ability and gradually increasing its

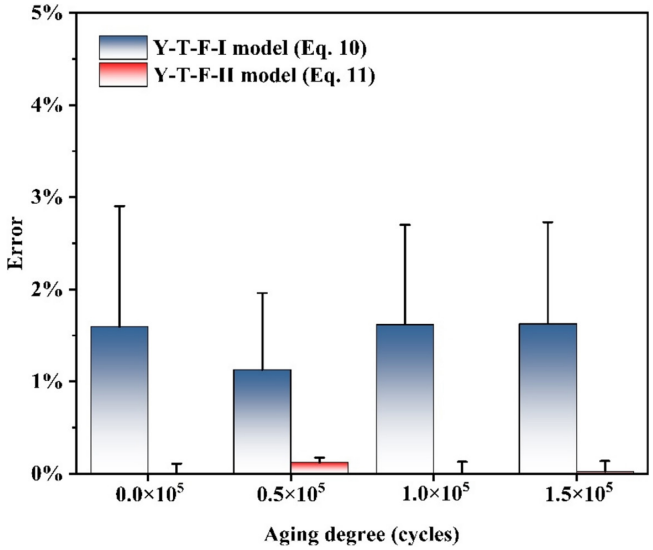

FIGURE 11 | Comparison of the prediction errors between the Y-T-F-I model (Equation 10) and the Y-T-F-II model (Equation 11). [Colour figure can be viewed at wileyonlinelibrary.com]

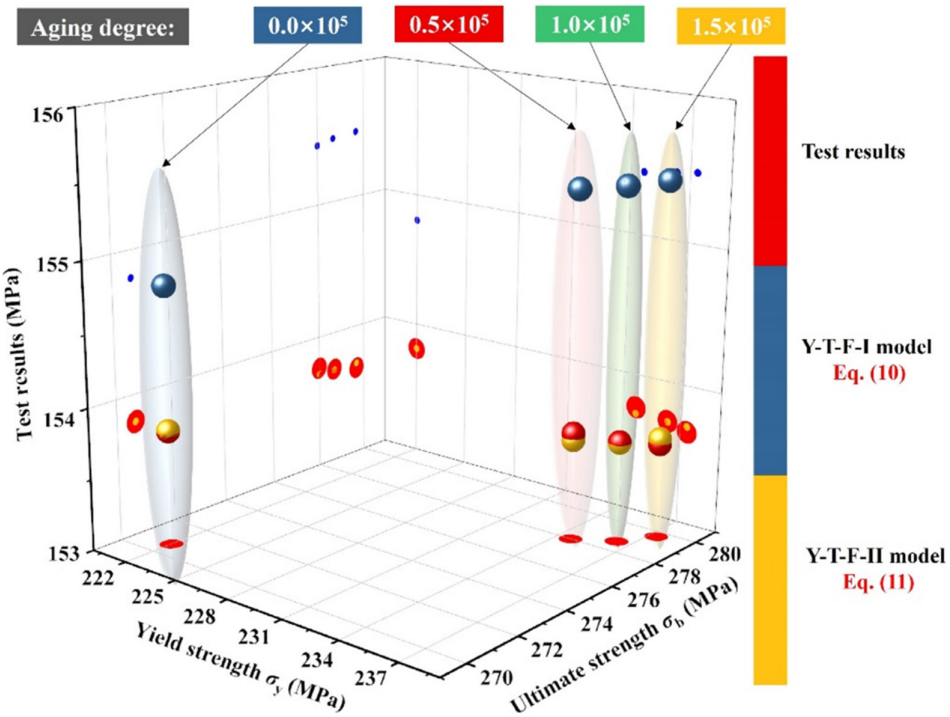

FIGURE 10 | Comparison of the predicted fatigue strength results between the Y-T-F-I model (Equation 10) and the Y-T-F-II model (Equation 11). [Colour figure can be viewed at wileyonlinelibrary.com]

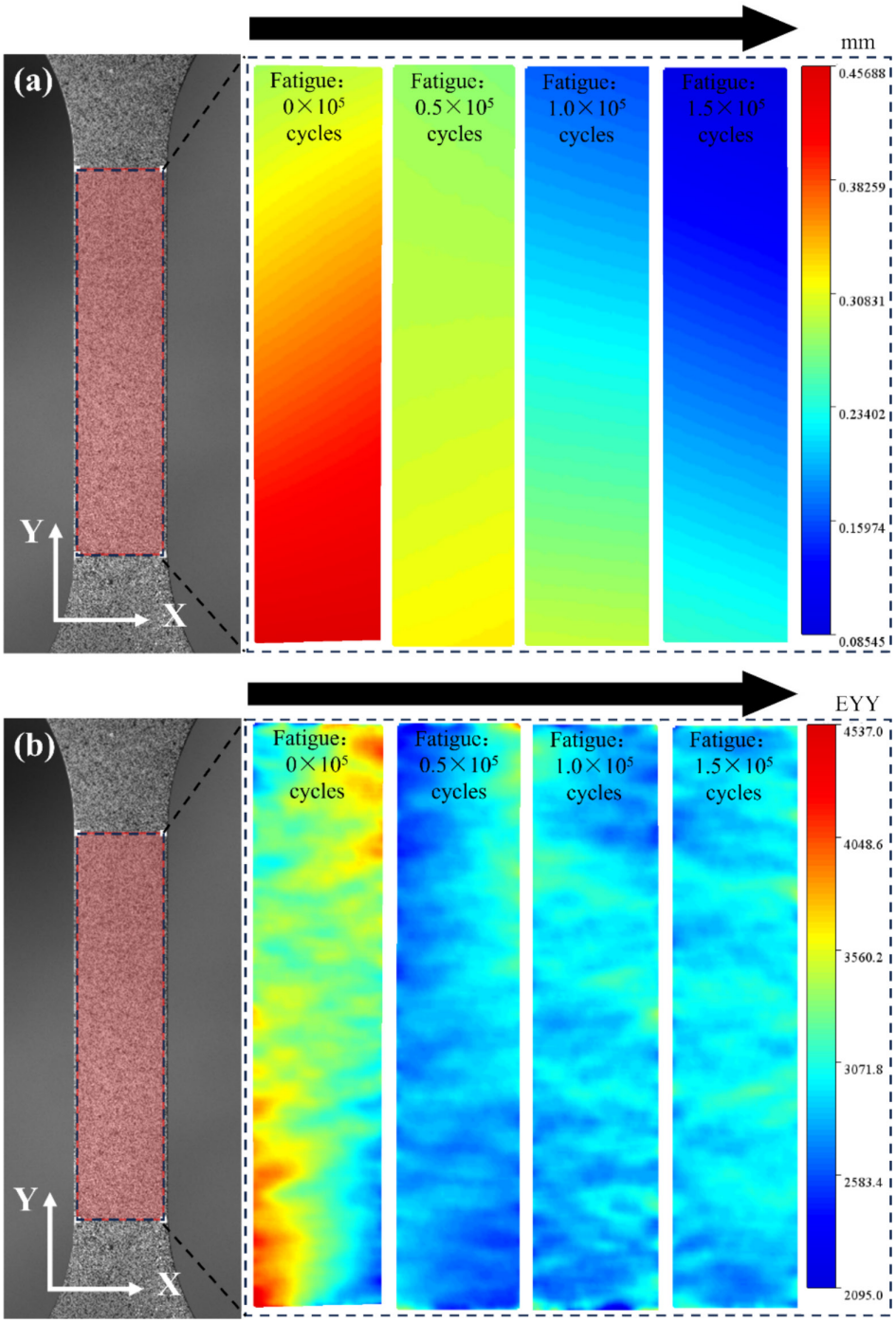

FIGURE 12 | Trend of single-cycle strain response on the sample surface under different aging states. (a) Total displacement. (b) *Y*-direction strain [Colour figure can be viewed at wileyonlinelibrary.com]

stiffness. In this case, the material exhibits a stronger resistance to deformation under the same load, leading to weakened displacement and strain responses.

4 | Conclusions

This study, using digital image correlation technology, provides an in-depth analysis of the evolution of the surface displacement field of 6005A-T6 aluminum alloy under different fatigue aging states and systematically investigates the changes in the material's mechanical properties. Based on this, a novel method is proposed to account for the influence of fatigue aging on material properties. We can draw the following conclusions:

1. As the number of fatigue cycles increases, the ultimate strength and yield strength of 6005A-T6 aluminum alloy slightly increase, while the reduction in area and elongation show a decreasing trend, indicating that the material's toughness and plasticity gradually weaken. The intensification of fatigue aging leads to the accumulation of

dislocation and defects within the material, which in turn affects its deformation ability and fatigue strength.

2. This study considers the influence of fatigue aging on the relationship between tensile and fatigue properties and proposes the Y-T-F-II model incorporating the aging function. Through comparative analysis, it was found that the Y-T-F-II model provides the best prediction of the fatigue strength of newly fabricated 6005A-T6 material, with a maximum error of 0.17%.

3. The surface strain responses of the samples under different aging (fatigue) states show that 6005A-T6 material gradually undergoes cyclic hardening, exhibiting a stronger resistance to deformation under the same load.

Nomenclature

σ_y	Yield strength
σ_b	Ultimate strength
Ψ	Section shrinkage
σ_w	Fatigue strength
A	Material constant
δ	Elongation
N^{pre}	Aging (fatigue) state
C, w	Fitted material parameters
σ_w^{pre}	Fatigue strength considering material fatigue aging
$\sigma_{w\text{-aging}}^{pre}$	Fatigue strength predicted by the Y-T-F-II model
$A(\alpha, \beta)$	Fatigue aging correction function
IPF	Inverse pole figure
BM	Base metal
Y-T-F model	Yield strength-tensile strength-fatigue strength model
Y-T-F-I/II model	Yield strength-tensile strength-fatigue strength-I/II model

Author Contributions

Bing Yang: writing – original draft preparation, resources, conceptualization. **Zhe Zhang:** writing – original draft preparation, data curation. **Hai Deng:** investigation. **Mingyang Ma:** supervision. **Jinbang Liu:** software. **Wenyang Shao:** investigation. **Chao Wang:** resources. **Shoune Xiao:** project administration. **Guangwu Yang:** validation. **Zhu Tao:** supervision.

Acknowledgments

The work was supported by the National Natural Science Foundation of China (52375159, 52175123) and the Fund of China Academy of Railway Sciences Corporation Limited (2022YJ309).

The authors thank Haoyu Zheng and Mian Huang for assistance with the experiment. In particular, the authors would like to thank Analysis and Testing Center of Southwest Jiaotong University for their assistance with SEM test.

Conflicts of Interest

The authors declare no conflicts of interest.

Data Availability Statement

The data that support the findings of this study are available from the corresponding author upon reasonable request.

References

1. Y. Tang, "Study on Stable Load Bearing Performance of Aluminum Alloy Pedestrian Truss Bridge" (master's diss., Chongqing Jiaotong University, 2022), https://doi.org/10.27671/d.cnki.gcjtc.2022.000557.

2. T. Siwowski, "Aluminium Bridges–Past, Present and Future," *Structural engineering international* 16, no. 4 (2006): 286–293, https://doi.org/10.2749/101686606778995137.

3. R. Coughlin, "Fatigue of Aluminum Welds in Canadian Highway Bridges" (master's diss., University of Waterloo, 2010), https://api.semanticscholar.org/CorpusID:110069203.

4. Z. Zhang, B. Yang, F. Feng, et al., "Multiaxial Fatigue Model Describing Crack Growth Behavior and Its Application in Welded Structures of Railway Frames," *International Journal of Fatigue* 194 (2025): 108831, https://doi.org/10.1016/j.ijfatigue.2025.108831.

5. C. Duan, X. Hao, X. Luo, X. Cao, H. Xu, and Z. Zhu, "Microstructure and Fatigue Properties of Laser-MIG Hybrid Welding of Medium-Thickness 6005A Aluminum Alloy," *Engineering Failure Analysis* 165 (2024): 108753, https://doi.org/10.1016/j.engfailanal.2024.108753.

6. Q. Zhang, C. Wang, G. Mi, W. Zhang, and J. Wang, "Influence of Compound Laser on Paint Removal Depth and Performance of 6005A Aluminum Alloy," *Journal of Materials Engineering and Performance* 23 (2024): 8666–8675, https://doi.org/10.1007/s11665-023-08557-2.

7. X. Wang, T. Zhu, L. Lu, et al., "Rate-Dependent Damage Sequence Interaction Model for Predicting the Mechanical Property of In-Service Aluminum Alloy 6005A-T6," *Mechanics of Materials* 191 (2024): 104959, https://doi.org/10.1016/j.mechmat.2024.104959.

8. L. Wu, B. Yang, X. Han, et al., "Improving Liquation Cracks and Mechanical Properties of 6005A Aluminum Alloy MIG Welded Joints via a Hybrid Milling-Friction Stir Processing Tool," *International Journal of Advanced Manufacturing Technology* 127 (2023): 419–429, https://doi.org/10.1007/s00170-023-11539-2.

9. L. Wu, X. Han, G. Ma, et al., "Effects of Welding Layer Arrangement on Microstructure and Mechanical Properties of Gas Metal Arc Welded 5083/6005A Aluminium Alloy Butt Joints," *Transactions of Nonferrous Metals Society of China* 33 (2023): 1665–1676, https://doi.org/10.1016/S1003-6326(23)66212-0.

10. Y. Cheng, J. K. Yan, F. Zhang, et al., "Surrogate Modeling of Pantograph-Catenary System Interactions," *Mechanical Systems and Signal Processing* 224 (2025): 112134, https://doi.org/10.1016/j.ymssp.2024.112134.

11. Ö. Karakaş and J. Szusta, "Monotonic and Low Cycle Fatigue Behaviour of 2024-T3 Aluminium Alloy Between Room Temperature and 300°C for Designing VAWT Components," *Fatigue & Fracture of Engineering Materials & Structures* 39 (2016): 95–109, https://doi.org/10.1111/ffe.12336.

12. C. S. Hattori, G. F. C. Almeida, R. L. P. Gonçalves, et al., "Microstructure and Fatigue Properties of Extruded Aluminum Alloys 7046 and 7108 for Automotive Applications," *Journal of Materials Research and Technology* 14 (2021): 2970–2981, https://doi.org/10.1016/j.jmrt.2021.08.085.

13. H. Wang, S. Yang, L. Han, S. Yu, S. Ren, and G. Zhang, "Effect of Prior Oxidation and Creep Damages on Subsequent Tensile Properties of Low Alloy Steels," *Materials Research Express* 6 (2019): 116515, https://doi.org/10.1088/2053-1591/ab44ea.

14. Z. Zhang, B. Yang, S. Wang, et al., "Mixed Mode (I/II) Fatigue Crack Growth in Butt-Welded Joints Using Actual Stress Intensity Factors,"

Theoretical and Applied Fracture Mechanics 138 (2025): 104894, https://doi.org/10.1016/j.tafmec.2025.104894.

15. C. Zhang, R. Wang, and G. Song, "Effects of Pre-Fatigue Damage on Mechanical Properties of Q690 High-Strength Steel," *Construction and Building Materials* 252 (2020): 118845, https://doi.org/10.1016/j.conbuildmat.2020.118845.

16. H. Chen, W. Li, W. Chen, et al., "Remnant Tensile and Creep Properties of Aluminized AISI 321 Austenite Stainless Steel Under Prior Creep–Fatigue Interaction," *Fatigue & Fracture of Engineering Materials & Structures* 45 (2022): 3746–3763, https://doi.org/10.1111/ffe.13832.

17. U. Sánchez-Santana, C. Rubio-González, G. Mesmacque, A. Amrouche, and X. Decoopman, "Dynamic Tensile Behavior of Materials with Previous Fatigue Damage," *Materials Science and Engineering: A* 497 (2008): 51–60, https://doi.org/10.1016/j.msea.2008.07.063.

18. X. Wang, T. Zhu, L. Lu, et al., "A Damage Sequence Interaction Model for Predicting the Mechanical Property of In-Service Aluminium Alloy 6005A-T6," *Engineering Fracture Mechanics* 291 (2023): 109565, https://doi.org/10.1016/j.engfracmech.2023.109565.

19. X. Wang, T. Zhu, J. Zhang, et al., "Prediction of Rate-Dependent Residual Strength of Aluminum Alloy of Car Body for In-Service High-Speed Trains," *Journal of Central South University (Science and Technology)* 55, no. 5 (2024): 2000–2010, https://doi.org/10.11817/j.issn.1672-7207.2024.05.030.

20. W. Li, Y. Sun, H. Zhang, L. Xu, and L. Wang, "Effect of Test Rate on Mechanical Properties of 6005A-T6 Aluminum Alloy," *Nonferrous Metals Processing* 51 (2022): 21–24, https://doi.org/10.3969/j.issn.1671-6795.2022.03.005.

21. Y. Peng, G. Wang, S. Pan, and Y. Rong, "6005A Aluminum Dynamic Mechanical Model Considering the Dynamic Recovery Process," *Journal of Mechanical Engineering* 50 (2014): 32–39, https://doi.org/10.3901/JME.2014.10.032.

22. W. Sun, Y. Jing, W. Tong, et al., "Dynamic Mechanical Property of 6005A-T6 Aluminum Alloy for Automotive Use," *Rare Metal Materials and Engineering* 50 (2021): 2118–2124, https://doi.org/10.12442/j.issn.1002-185X.20200495.

23. S. Zhou, B. Yang, C. Wang, et al., "Fatigue Crack Growth Rate Estimation of 6005A-T6 Aluminum Alloys with Different Stress Ratios Using Machine Learning Methods," *Chinese Journal of Nonferrous Metals* 33 (2023): 2416–2427 https://doi.org/10.11817/j.ysxb.1004.0609.2022-43508.

24. F. Feng, T. Zhu, B. Yang, S. Zhou, and S. Xiao, "A Physics-Informed Neural Network Approach for Predicting Fatigue Life of SLM 316L Stainless Steel Based on Defect Features," *International Journal of Fatigue* 188 (2024): 108486, https://doi.org/10.1016/j.ijfatigue.2024.108486.

25. S. Zhou, B. Yang, K. Lv, et al., "Elastic- Plastic Simulation Study on 6005A Aluminum Alloy Crack Propagation Based on XFEM," *International Journal of Applied Mechanics* 17, no. 1 (2025): 2450126, https://doi.org/10.1142/S1758825124501266.

26. Y. Sato and Y. Jiao, "Strain Amplitude Dependency of Cyclic Hardening/Softening Behavior of 490 N/mm2 Class Steel," *Journal of Constructional Steel Research* 222 (2024): 108988, https://doi.org/10.1016/j.jcsr.2024.108988.

27. K. Dinesh, B. Dash, R. Kannan, . H Krishnaswamy, S Sankaran "Effect of Strain Amplitude on the Low Cycle Fatigue Behavior and Deformation Mechanisms in Alloy SU-263 at Elevated Temperature," *Materials Science and Engineering: A* 920 (2024): 147518, https://doi.org/10.1016/j.msea.2024.147518.

28. L. Sun, X. Zhang, K. Li, et al., "Creep-Fatigue Damage Level Evaluation Based on the Relationship Between Microstructural Evolution and Mechanical Property Degradation," *International Journal of Plasticity* 181 (2024): 104086, https://doi.org/10.1016/j.ijplas.2024.104086.

29. J. Pang, S. Li, Z. Wang, and Z. Zhang, "Relations Between Fatigue Strength and Other Mechanical Properties of Metallic Materials," *Fatigue & Fracture of Engineering Materials & Structures* 37 (2014): 958–976, https://doi.org/10.1111/ffe.12158.

30. R. Liu, P. Zhang, Z. J. Zhang, B. Wang, and Z. F. Zhang, "A Practical Model for Efficient Anti-Fatigue Design and Selection of Metallic Materials: I. Model Building and Fatigue Strength Prediction," *Journal of Materials Science & Technology* 70 (2021): 233–249, https://doi.org/10.1016/j.jmst.2020.08.038.

31. R. Liu, P. Zhang, Z. J. Zhang, B. Wang, and Z. F. Zhang, "A Practical Model for Efficient Anti-Fatigue Design and Selection of Metallic Materials: II. Parameter Analysis and Fatigue Strength Improvement," *Journal of Materials Science & Technology* 70 (2021): 250–267, https://doi.org/10.1016/j.jmst.2020.08.037.

32. C. X. Shi, Q. P. Zhong, and C. G. Li, "China Materials Engineering Canon," in *Fundamentals of Materials Engineering*, vol. 1 (Chemical Industry Press, 2005).

33. P. G. Forrest, *Fatigue of Metals* (Pergamon Press, 1962).

34. J. Li, Q. Sun, Z. P. Zhang, C. Li, and Y. Qiao, "Theoretical Estimation to the Cyclic Yield Strength and Fatigue Limit for Alloy Steels," *Mechanics Research Communications* 36 (2009): 316–321, https://doi.org/10.1016/j.mechrescom.2008.10.011.

35. D. Ye and Z. Wang, "A New Approach to Low-Cycle Fatigue Damage Based on Exhaustion of Static Toughness and Dissipation of Cyclic Plastic Strain Energy During Fatigue," *International Journal of Fatigue* 23 (2001): 679–687, https://doi.org/10.1016/S0142-1123(01)00027-5.

36. J. C. Pang, S. X. Li, Z. G. Wang, and Z. F. Zhang, "General Relation Between Tensile Strength and Fatigue Strength of Metallic Materials," *Materials Science and Engineering: A* 564 (2013): 331–341, https://doi.org/10.1016/j.msea.2012.11.103.

37. J. A. Bannantine, J. J. Comer, and J. L. Handrock, *Fundamentals of Metal Fatigue Analysis* (Prentice Hall, 1990).

38. C. K. Lin, P. K. Lai, and T. S. Shih, "Influence of Microstructure on the Fatigue Properties of Austempered Ductile Irons—I. High-cycle fatigue," *International Journal of Fatigue* 18 (1996): 297–307, https://doi.org/10.1016/0142-1123(96)82895-7.

39. K. Lv Study on Crack Propagation Behavior of 6005A-T6 Aluminum Alloy Laser-MIG Hybrid Welded Joint. (Southwest Jiaotong University, 2024).

40. GB/T 228.1-2021, *Tensile Testing of Metallic Materials-Part 1: Room Temperature Test Methods* (China Standard Press, 2021).

41. R. J. Sanford and J. W. Dally, "A General Method for Determining Mixed-Mode Stress Intensity Factors From Isochromatic Fringe Patterns," *Engineering Fracture Mechanics* 11 (1979): 621–633, https://doi.org/10.1016/0013-7944(79)90123-1.

42. D. Ye, "Deleterious Effects of Low-Cycle Fatigue on Static Mechanical Properties of an Aircraft Aluminum Alloy and Damage Characterization Based on Macroscopic CDM Method/Microscopic GTN Model," *International Journal of Fatigue* 193 (2025): 108793, https://doi.org/10.1016/j.ijfatigue.2024.108793.

43. F. Stangenberg, R. Breitenbücher, O. T. Bruhns,et al., *Lifetime-Oriented Structural Design Concepts* (Springer Berlin, 2009), https://doi.org/10.1007/978-3-642-01462-8_3.

44. J. Lemaitre and R. Desmorat, *Engineering Damage Mechanics (Ductile, Creep, Fatigue and Brittle Failures)*, first ed. (Springer-Verlag, 2005), https://doi.org/10.1007/b138882.

45. D. Ye and Z. Wang, "A New Approach to Low-Cycle Fatigue Damage Based on Exhaustion of Static Toughness and Dissipation of Cyclic Plastic Strain Energy During Fatigue," *International Journal of Fatigue* 27 (2001): 1102–1114, https://doi.org/10.1016/S0142-1123(01)00027-5.

46. G. Cheng and A. Plumtree, "A Fatigue Damage Accumulation Model Based on Continuum Damage Mechanics and Ductility Exhaustion,"

International Journal of Fatigue 20 (1998): 495–501, https://doi.org/10.1016/S0142-1123(98)00018-8.

47. D. Ye, Y. Xu, L. Xiao, and H. Cha, "Effects of Low-Cycle Fatigue on Static Mechanical Properties, Microstructures and Fracture Behavior of 304 Stainless Steel," *Materials Science and Engineering: A* 527 (2010): 4092–4102, https://doi.org/10.1016/j.msea.2010.03.027.

48. D. Ye, "Effect of Cyclic Straining at Elevated-Temperature on Static Mechanical Properties, Microstructures And Fracture Behavior of Nickel-Based Superalloy GH4145/SQ," *International Journal of Fatigue* 27 (2005): 1102–1114, https://doi.org/10.1016/j.ijfatigue.2005.01.014.

49. U. Sánchez-Santana, C. Rubio-González, G. Mesmacque, A. Amrouche, and X. Decoopman, "Effect of Fatigue Damage on the Dynamic Tensile Behavior of 6061-T6 Aluminum Alloy and AISI 4140T Steel," *International Journal of Fatigue* 31 (2009): 1928–1937, https://doi.org/10.1016/j.ijfatigue.2008.03.011.

50. A. Wöhler, "Versuche uber biegung und verdrehung von eisenbahnachscn wahrent der fahrt," *Z. Bauwesen* 8 (1858): 641.

51. J. Fan, Z. Wang, C. Liu, D. Shi, and X. Yang, "A Tensile Properties-Related Fatigue Strength Predicted Machine Learning Framework for Alloys Used in Aerospace," *Engineering Fracture Mechanics* 301 (2024): 110057, https://doi.org/10.1016/j.engfracmech.2024.110057.

52. R. Liu, Y. Z. Tian, Z. J. Zhang, P. Zhang, X. H. An, and Z. F. Zhang, "Exploring the Fatigue Strength Improvement of Cu-Al Alloys," *Acta Materialia* 144 (2018): 613–626, https://doi.org/10.1016/j.actamat.2017.11.019.

53. X. H. An, S. D. Wu, Z. G. Wang, and Z. F. Zhang, "Enhanced Cyclic Deformation Responses of Ultrafine-Grained Cu and Nanocrystalline Cu–Al Alloys," *Acta Materialia* 74 (2014): 200–214, https://doi.org/10.1016/j.actamat.2014.04.053.

54. X. H. An, Q. Y. Lin, S. D. Wu, and Z. F. Zhang, "Improved Fatigue Strengths of Nanocrystalline Cu and Cu–Al Alloys," *Materials Research Letters* 3 (2015): 135–141, https://doi.org/10.1080/21663831.2015.1029645.